Astronomy & Astrophysics manuscript no. output
July 27, 2026

Rotation of ZZ Ceti stars as seen by TESS II. New data sets, new methods

Zsófia Bognár⋆, Ádám Sódor

Konkoly Observatory, HUN-REN Research Centre for Astronomy and Earth Sciences, MTA Centre of Excellence, Konkoly Thege Miklós út 15-17, 1121 Budapest, Hungary

ABSTRACT

Context. ZZ Ceti stars provide a valuable opportunity to study white dwarf rotation through rotationally split pulsation modes. Space-based photometry has also revealed outburst phenomena in some cool ZZ Ceti stars, although the occurrence and properties of these events remain poorly understood.

Aims. We aim to extend the search for rotationally split pulsation triplets and outburst-like brightenings among known ZZ Ceti stars observed by TESS.

Methods. We analysed 120 s and 20 s cadence TESS light curves of Sectors 1 through 96. After light-curve correction, sector-quality filtering, and outlier rejection, we performed frequency analysis and iterative prewhitening. Candidate rotationally split triplets were identified with an automated pipeline that searches for nearly symmetric frequency triples, groups them into clusters with similar splittings, and ranks the clusters using internal quality metrics. The accepted triplets were selected by final visual validation. Rotation periods were estimated from the mean frequency splittings. Outburst candidates were identified from corrected light curves using smoothed flux variations relative to local baselines, followed by visual inspection.

Results. We identify 11 ZZ Ceti stars with accepted triplet candidates and derive rotation periods ranging from about 8 to 94 h. The targets mostly occupy the normal white dwarf mass range and are broadly consistent with the dispersion of rotation periods reported in previous studies. We also identify 11 stars showing outburst-like brightenings. The candidate events are generally short, with median durations of about 0.3–1.9 h. Four repeated events are detected in TIC 219442838 and two in TIC 800153845, supporting their interpretation as genuine outbursts. Some candidates appear hotter than previously known outbursting ZZ Ceti stars, suggesting that outburst-like behaviour may extend beyond the coolest DAVs; however, spectroscopic confirmation and follow-up photometry are required.

Key words. techniques: photometric – stars: oscillations – white dwarfs

1. Introduction

ZZ Ceti (or DAV) stars constitute the most populous class of pulsating white dwarfs. These low-to-mid radial-order g-mode pulsators generally show relatively low-amplitude variability ($A \sim 0.1\%$) in the $100-1500$ s period range. The $\kappa-\gamma$ mechanism (Dolez & Vauclair 1981; Winget et al. 1982) in combination with the convective driving mechanism (Brickhill 1991; Goldreich & Wu 1999) is responsible for the excitation of the observed pulsations.

Their behaviour can be well understood in terms of their location within the instability strip during their cooling evolution. When entering the hot, blue edge of the empirical instability strip, they exhibit only a few low-amplitude brightness variations with short pulsation periods. We note that these pulsation modes are more stable in time than those observed in cooler DAVs, making them suitable for precise pulsation-period measurements and, in some cases, even for detecting evolutionary, secular period changes. As the star cools, however, the observed amplitudes increase, and more modes become detectable. In many cases, these modes are not stable in time: amplitude and frequency variations are observed, which complicate the determination of pulsation frequencies using standard pre-whitening processes. The pulsation properties observed in different parts of the instability strip are well summarised by Hermes et al. (2017).

Two phenomena that are discussed later in this paper should be mentioned here. The first is rotational frequency splitting. Rotation lifts the azimuthal degeneracy of non-radial modes, producing multiplets whose frequency separations depend on the rotation rate in the layers probed by the corresponding pulsation modes. In pulsating white dwarfs, we can usually observe only modes with horizontal degrees $\ell = 1$ and 2, whose multiplets appear as triplets and quintuplets, respectively. In this paper, we search for multiplet frequencies in order to determine the stellar rotation periods. That is, we continued our work presented first in Bognár & Sódor (2024), hereafter Paper I, but with more data sets and a more systematic splitting-search pipeline. Instead of inspecting Lomb-Scargle periodograms by eye as the primary search method, we first generated pre-whitened frequency lists for all light curves, automatically searched them for symmetric triplet patterns, grouped candidates with similar splittings into clusters, ranked the clusters using internal quality metrics, and only then performed the final visual validation.

More broadly, the motivation for searching for multiplets is that white dwarf rotation rates, especially as a function of stellar mass, can provide insight into the angular-momentum transport mechanisms operating in their progenitors, including the coupling between red-giant cores and envelopes (Hermes et al. 2017). Further discussion can be found in Kawaler (2003), Kawaler (2015), and Córsico et al. (2019).

⋆ e-mail: bognar.zsofia@csfk.org

The second noteworthy phenomenon is associated with cool ZZ Ceti stars: the presence of so-called outbursts in their light curves. During an outburst, the mean brightness of the star increases by a few percent on an approximately hourly timescale. The star then remains in this brightened state for several hours before fading back to its original brightness. The recurrence of outbursts does not follow a regular pattern: they may recur after days or weeks, but longer intervals are also possible (Bognár et al. 2023). For more information on different outbursting stars, see the papers of Bell et al. (2015, 2016, 2017) and Hermes et al. (2015). From a theoretical point of view, outbursts may be caused by non-linear mode coupling, radiative damping, or phase shifts of travelling waves reflected from the outer turning point close to the convection zone; see, for example, Bell et al. (2017), Luan & Goldreich (2018), and Montgomery et al. (2020).

The present study is based on observations obtained by the Transiting Exoplanet Survey Satellite (TESS). Launched on 18 April 2018, TESS made it possible to observe selected short-period pulsators with a 120-second cadence. The 2020 – 2022 Extended Mission provided an even more valuable observing mode: 20-second cadence data became available, proving particularly suitable for the study of pulsating white dwarfs. Studies of pulsating white dwarfs and subdwarfs observed by TESS are coordinated by the TESS Asteroseismic Science Consortium Compact Pulsators Working Group (TASC WG#8).

The first paper in this series, published in 2024, focused on the rotation of ZZ Ceti stars using TESS data. The present paper is a continuation of that work, incorporating data from newly observed sectors. In addition to searching for multiplets indicative of stellar rotation, we also search for possible outburst candidates. These tasks were largely automated, as described in the following sections.

2. The TESS data sets

This section describes the construction of the TESS data set and the main processing steps applied before the frequency analysis. The goal was to obtain a homogeneous set of corrected light curves and frequency lists suitable for the automated triplet search.

The main steps of the complete analysis pipeline, from the downloaded TESS light-curve files to the final accepted rotational triplets, are summarised in Fig. 1.

2.1. Data acquisition

Our aim was not to search for new ZZ Ceti stars. We therefore compiled our target list from three published samples: Table 4 of Bognár & Sódor (2016), which lists 170 ZZ Ceti stars; the sample of 75 DAVs presented by Romero et al. (2022); and the most recent catalogue of 32 new TESS ZZ Ceti stars published by Romero et al. (2025). This resulted in a total sample of 277 stars.

TESS observed 239 of these targets. We used light curve data products generated by the TESS Science Processing Operations Center (SPOC) pipeline (Jenkins et al. 2016). For all 239 stars, 120 s cadence data are available; for 178 of them, 20 s cadence observations are also available, while 61 stars have only 120 s cadence data. We downloaded all available TESS light curves up to Sector 96, corresponding to the end of Cycle 7.

The TESS light-curve FITS products of the SPOC pipeline were downloaded from the Mikulski Archive for Space Telescopes[1] (MAST). We adopted the systematics-corrected `PDCSAP_FLUX` values as the starting point of our analysis. We obtained 2201 valid TESS light-curve FITS files for 239 stars; 1343 in the 120 s cadence and 858 in the 20 s cadence.

2.2. Light curve preparation

The individual sector light curves were corrected for long-term trends. We applied different correction-window parameters for the two cadences: 200 data points for the 120 s data and 1000 for the 20 s data.

We omitted 18 of the 2201 sector data points due to extensive scatter. The corrected sector light curves were then merged separately for each target and cadence. This resulted in 239 combined 120 s light curves and 178 combined 20 s light curves, giving a total of 417 corrected TESS light curves.

2.3. Frequency analysis

After the corrected sector light curves had been merged, we performed a Fourier analysis and iterative pre-whitening on all combined light curves. The analysis was carried out with a custom Python script based on Lomb-Scargle periodograms and iterative sinusoidal fitting. In each step, the highest-amplitude significant frequency was identified, fitted, and subtracted from the light curve. The iteration was stopped when no peak exceeded the adopted false-alarm probability threshold of 0.1 percent, or when the maximum number of 99 extracted frequencies was reached.

The analysis was performed separately for the 120 s and 20 s cadence data. We used maximum search frequencies of $360\,\mathrm{d}^{-1}$ and $900\,\mathrm{d}^{-1}$ for the 120 s and 20 s data, respectively. For each light curve, we saved the extracted frequency list, the residual light curve after pre-whitening, and the initial Lomb-Scargle periodogram before any frequencies were removed.

In a subsequent quality-control step, unusually noisy sectors and outlier data points were identified from the residual light curves using robust scatter diagnostics and were excluded before performing a second iteration of the frequency analysis.

3. Searching for triplets

We searched for rotationally split triplets using the frequency lists obtained from the final pre-whitening analysis. In total, 417 frequency lists were analysed, corresponding to 239 light curves with 120 s cadence and 178 light curves with 20 s cadence. The search was automated to make the first candidate selection reproducible, but the final acceptance of triplets was still based on visual inspection.

The search was restricted to frequencies above $25\,\mathrm{d}^{-1}$, and only the 20 highest-amplitude frequencies from each list were used to reduce the number of chance combinations. The algorithm then searched for nearly symmetric frequency triples

$$f_1,\ f_2,\ f_3$$

satisfying

$$f_2 - f_1 \simeq f_3 - f_2.$$

The mean frequency separation of a candidate triplet is defined as

$$\Delta f = \frac{1}{2}\left[(f_2 - f_1) + (f_3 - f_2)\right].$$

[1] https://archive.stsci.edu/

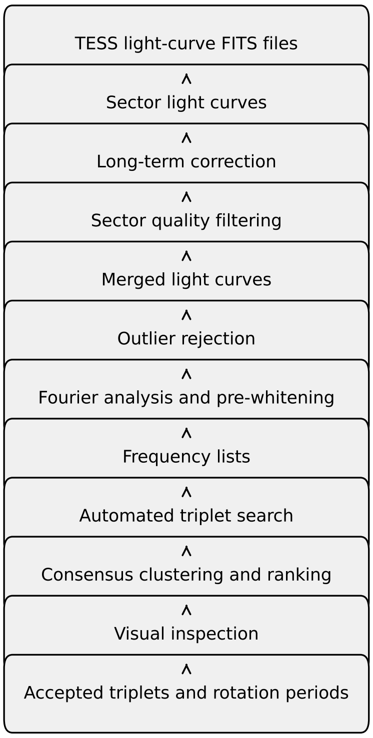

Fig. 1. Schematic overview of the analysis pipeline used to identify rotationally split triplets in the TESS light curves.

Candidate triplets with similar splittings were grouped into consensus clusters and ranked. This step helped to distinguish cases where several modes suggested the same rotational splitting from isolated, accidental frequency triples.

The automated search identified triplet candidates in 44 frequency lists, corresponding to 30 TIC targets. These candidates were inspected visually using frequency-amplitude diagrams and zoomed periodograms. Closely spaced alternative peaks were treated as competing detections of the same triplet component, and the highest-amplitude peak was retained. The final accepted sample contains 11 stars. Thus, the triplet search can be summarised as 417 analysed frequency lists, 44 frequency lists with automated triplet candidates, 30 candidate TIC targets, and 11 accepted rotators after visual validation (Fig. 2).

We summarised our findings in several tables. Table 1 shows the journal of observations of the pulsators exhibiting triplet structures. The temporal distribution of the observations of these 11 targets are visualised in Fig. 3. The accepted triplet frequencies and their separations are listed in Table 2. Finally, Table 3 summarises the average frequency splittings of the 11 stars showing triplet structures. We also listed the corresponding rotational periods, the mass of the stars, and in the comments, we can find whether a star is a newly found rotator or is already listed in Paper I, Romero et al. (2022) (R22) or in Romero et al. (2025) (R25). In these latter cases, we denoted the rotation period values found in these previous papers.

The final visually accepted triplets are presented in Figs. 4 and 5. The panels show the local frequency-amplitude structure around each selected triplet and provide visual confirmation for the component identifications used in Table 2. In cases where both 120 s and 20 s cadence data were available, the agreement between the independently analysed data sets supports the adopted splitting.

As in Paper I, we plotted the stellar mass as a function of the rotation period for the accepted triplet candidates in Fig. 6. Our new results are shown as filled black circles. We also included the 13 rotators from Paper I for which Gaia EDR3 white dwarf catalogue masses were available; these are shown as open triangles. For comparison, we plotted the isolated pulsating white dwarfs from Hermes et al. (2017) (their Table 4) as open circles, excluding EPIC 201730811 as in their original figure because it is a close post-common-envelope binary and retaining only objects with a Gaia EDR3 hydrogen-atmosphere photometric mass. The horizontal axis shows the rotation period in hours on a logarithmic scale, and the vertical axis shows the stellar mass in solar units. Thus, all masses shown in the figure are taken consistently from the Gaia EDR3 white dwarf catalogue.

The comparison with the Hermes et al. (2017) sample illustrates the previously noted tendency that the most massive white dwarfs appear to rotate faster. Our newly identified rotators do not include very high-mass objects, and therefore, they do not strongly test this trend at the high-mass end. Within our lower-mass sample, the points show substantial scatter and may even suggest longer rotation periods toward higher masses. However, given the small number of objects, the limited mass range, and the uncertainties inherent in deriving rotation periods from a small number of multiplets, we do not interpret this as evidence for an opposite correlation. Rather, our results are broadly consistent with the large dispersion seen among normal-mass white dwarfs in the Hermes et al. (2017) sample.

4. Investigation of outburst candidates

We searched for outburst-like brightenings in the corrected TESS light curves, treating the 120 s and 20 s cadence data sets separately. Before the search, we removed problematic sectors identified from the sector-quality diagnostics and applied an iterative outlier rejection using an 8 MAD threshold in order to suppress isolated deviant points without removing genuine multi-hour brightenings. The outburst search was deliberately conservative: it was designed to identify a robust candidate sample rather than to measure a complete occurrence rate.

MAD stands for median absolute deviation. It is defined as

$$\mathrm{MAD} = \mathrm{median}\left(|x_i - \mathrm{median}(x)|\right).$$

First, the median of the data set is calculated. Then the absolute deviation of each data point from this median is computed, and the median of these deviations gives the MAD. It is a robust measure of scatter because it is much less sensitive to outliers than the standard deviation. In our analysis, the 8 MAD threshold means that isolated points lying far from the typical scatter of the light curve were rejected as outliers.

The automatic outburst search was based on the time-domain behaviour of the corrected fluxes. We first identified contiguous groups of points lying more than 3 MAD above the median level of the light curve. To reject low-level fluctuations and isolated excursions, a group was kept only if its maximum point exceeded 5 MAD, if it contained enough consecutive high points for the corresponding cadence, and if its duration was shorter than 0.30 d. This upper duration limit is longer than the individual events ultimately measured here, but it excludes broad residual trends that are unlikely to be classical outburst profiles. The automatic candidates were then ranked using a score that combines the peak significance, the number of high points, and the integrated excess above the local baseline.

For the final duration measurements we used a separate, local procedure. Around each candidate event, we estimated

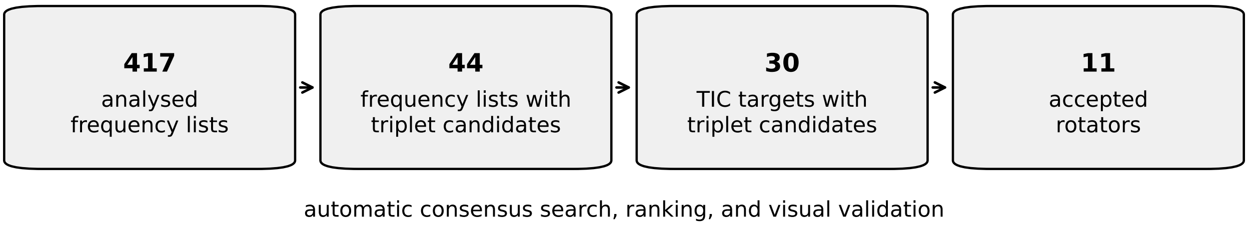

Fig. 2. Workflow summary of the rotational-triplet search. The numbers show the reduction from all analysed frequency lists to the final visually accepted rotators.

Table 1. TESS data used for the accepted triplet candidates. N is the number of data points after cleaning the light curve, ΔT is the total length of the data sets including gaps, and the sector labels indicate the cadence: S denotes 120 s cadence data, while US denotes 20 s ultrashort-cadence data. The listed CROWDSAP value is the median of the sector values. The CROWDSAP keyword represents the ratio of the target flux to the total flux in the TESS aperture.

TIC ID	Start time (BJD−2457000)	N	ΔT (d)	G mag	Sector (US: 20 s, S: 120 s)	CROWDSAP
101014997	1385.938	59708	784.008	15.064	S3–4, S30–31	0.921
101014997	2115.887	191458	54.060	15.064	US30–31	0.919
11626063	1683.358	60777	1849.822	15.149	S14, S41, S54, S81	0.075
149863849	2361.777	49616	1493.320	13.556	S39, S66, S93	0.146
149863849	2361.776	289393	1493.318	13.556	US39, US66, US93	0.146
199666369	2390.654	2585915	1272.173	12.291	US40–41, US47–60, US73–86	0.976
217329125	2825.262	207304	759.118	15.777	US56, US83	0.935
262872628	2333.857	509050	1521.147	13.443	US38–39, US65–66, US93	0.710
287926830	2825.261	308895	759.118	15.962	US56, US82–83	0.191
313109945	1683.352	167583	1085.625	18.591	S14–15, S20–22, S40–41, S47–48, S53	0.077
313109945	2390.651	506832	378.326	18.591	US40–41, US47–48, US53	0.077
343296348	1629.139	75537	2225.498	15.869	S12–13, S39, S66, S93	0.394
343296348	2361.774	265161	1492.863	15.869	US39, US66, US93	0.394
394015496	1325.300	73551	2555.689	15.811	S1, S27–28, S67, S94	0.256
394015496	2061.855	246532	1819.135	15.811	US28, US67, US94	0.256
55650407	2036.278	2582841	1896.846	14.991	US27–39, US61–69, US87–89, US93–96	0.968

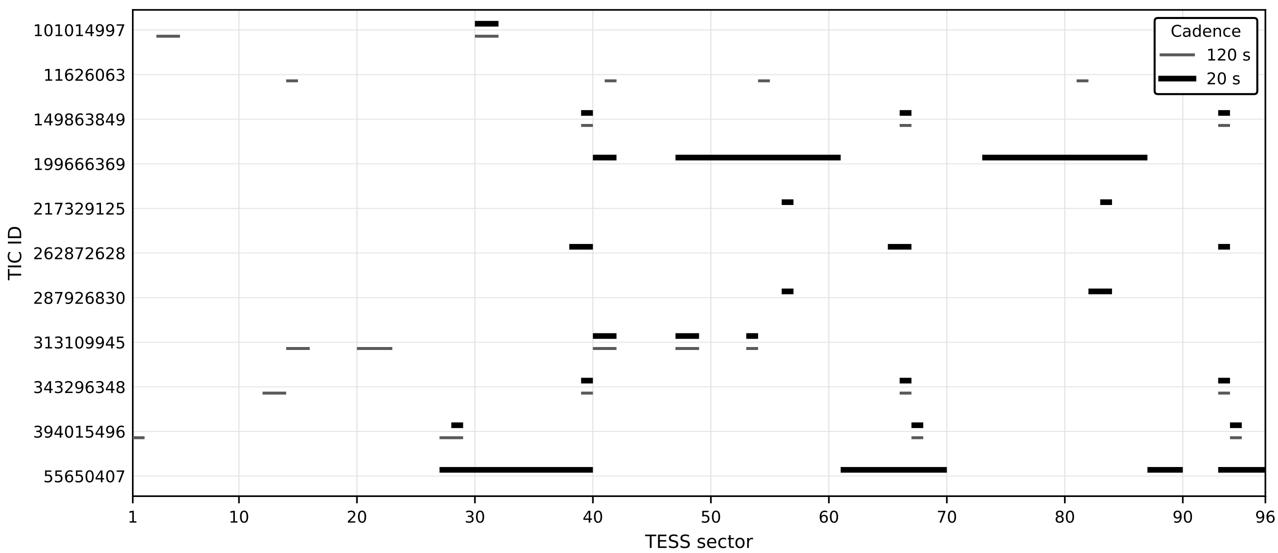

Fig. 3. TESS sector coverage of the 11 accepted triplet rotators. Each horizontal row corresponds to one TIC target, and the horizontal axis gives the TESS sector number, with tick marks indicating the beginning of the labelled sectors. Line segments mark sectors for which usable data were available. Thin grey segments denote 120 s cadence observations, while thick black segments denote 20 s cadence observations; the two cadences are plotted with a small vertical offset within each row to avoid overlap.

Table 2. Accepted triplet frequencies and frequency separations.

TIC ID	Frequencies [μHz]	Separations [μHz]	Mean Δf [μHz]
101014997 (120 s)	1605.944, 1618.399, 1630.772	12.454, 12.374	12.414
101014997 (20 s)	1605.948, 1618.372, 1630.776	12.424, 12.405	12.414
11626063 (120 s)	3901.163, 3902.746, 3904.284	1.583, 1.538	1.560
149863849 (120 s)	1477.824, 1496.014, 1514.247	18.191, 18.233	18.212
149863849 (20 s)	1477.808, 1496.003, 1514.213	18.195, 18.209	18.202
199666369 (20 s)	9134.726, 9150.865, 9167.004	16.139, 16.139	16.139
217329125 (20 s)	3892.313, 3897.760, 3903.246	5.447, 5.486	5.466
262872628 (20 s)	5178.871, 5191.850, 5204.841	12.978, 12.991	12.985
287926830 (20 s)	3612.840, 3618.345, 3623.914	5.505, 5.570	5.537
313109945 (120 s)	3345.665, 3347.356, 3349.048	1.691, 1.692	1.691
313109945 (20 s)	3345.665, 3347.356, 3349.048	1.691, 1.692	1.692
343296348 (120 s)	3468.955, 3475.054, 3481.169	6.099, 6.115	6.107
343296348 (20 s)	3468.954, 3475.070, 3481.170	6.116, 6.100	6.108
394015496 (120 s)	3223.004, 3228.026, 3233.048	5.022, 5.021	5.022
394015496 (20 s)	3222.972, 3228.027, 3233.048	5.054, 5.021	5.038
55650407 (20 s)	4983.652, 4997.882, 5012.106	14.230, 14.224	14.227

Table 3. Mean frequency splittings and estimated rotation periods for the accepted triplet candidates. The rotation periods were calculated assuming $C_{k,\ell} = 0.47$ and are listed without formal error bars. The masses were adopted from the Gaia EDR3 white dwarf catalogue (Gentile Fusillo et al. 2021), using the hydrogen-atmosphere photometric solutions.

TIC ID	$\langle \Delta f \rangle$ (μHz)	$P_{\rm rot}$ (h)	Mass ($M_\odot$)	Cadence	Comment	Literature $P_{\rm rot}$ (h)
101014997	12.414	11.86	0.623	120 s and 20 s	Paper I	11.9
11626063	1.560	94.35	0.597	120 s	new	
149863849	18.207	8.09	0.657	120 s and 20 s	R25	14.49-22.73
199666369	16.139	9.12	0.783	20 s	Paper I	9.1
217329125	5.466	26.93	0.614	20 s	new	
262872628	12.985	11.34	0.674	20 s	Paper I	12.2
287926830	5.537	26.59	0.572	20 s	new	
313109945	1.692	87.03	0.410	120 s and 20 s	Paper I	85.5
343296348	6.108	24.10	0.586	120 s and 20 s	R25	12.35
394015496	5.030	29.27	0.607	120 s and 20 s	Paper I	29.4
55650407	14.227	10.35	0.574	20 s	R25	12.12

the quiescent baseline from the median flux outside the event and estimated the local scatter as 1.4826 MAD, which is the Gaussian-equivalent robust standard deviation. The light curve was smoothed with a 0.25 h running mean before measuring the event width. This smoothing scale is much longer than the 20 s and 120 s cadences, so it suppresses point-to-point noise and short pulsation-cycle fluctuations, but it is still shorter than the hour-scale brightenings that we aimed to measure. The duration was defined as the interval over which the smoothed light curve remained above the local threshold baseline + 3σ. This definition gives a reproducible, conservative width for each event; it should be regarded as the duration of the high-confidence brightened part of the light curve rather than necessarily the full physical outburst duration.

The automatic search produced 39 event candidates in 13 TIC targets. After visual inspection of the local light curves, sector context, and smoothed profiles, we retained 19 events in 11 stars for Fig. 7 and Fig. 8. Thus, about half of the automatic triggers were rejected at the validation stage, mostly because they were too close to residual trends, sector-boundary features, or ambiguous low-amplitude variability. The visual rejection fraction provides an empirical indication that the automatic thresholding alone is not sufficient, and that the final sample should be interpreted as a conservative candidate sample.

After this automatic search and visual inspection, we retained 11 stars as outburst candidates: TIC 0001116746, 101901770, 1103347368, 219442838, 307908863, 366681966, 630426257, 67441210, 800153845, 800562727, and 842051075. These candidates indicate that outburst-like behaviour is present in a subset of the analysed ZZ Ceti stars, although individual detections should be interpreted with caution because of the heterogeneous TESS coverage and possible residual systematics. The journal of observations for these stars can be found in Table 4.

We note that one object in our outburst-candidate sample, TIC 366681966 (WD 1149+057), is already known as an outbursting ZZ Ceti star and was included in the sample of Bell et al. (2017). Thus, among the 11 outburst candidates identified here, ten are new candidates, while one corresponds to a previously known outbursting DAV.

5. Discussion

The two parts of our analysis probe different aspects of ZZ Ceti variability and are affected by different observational biases. We therefore discuss the rotational-triplet results and the outburst candidates separately below.

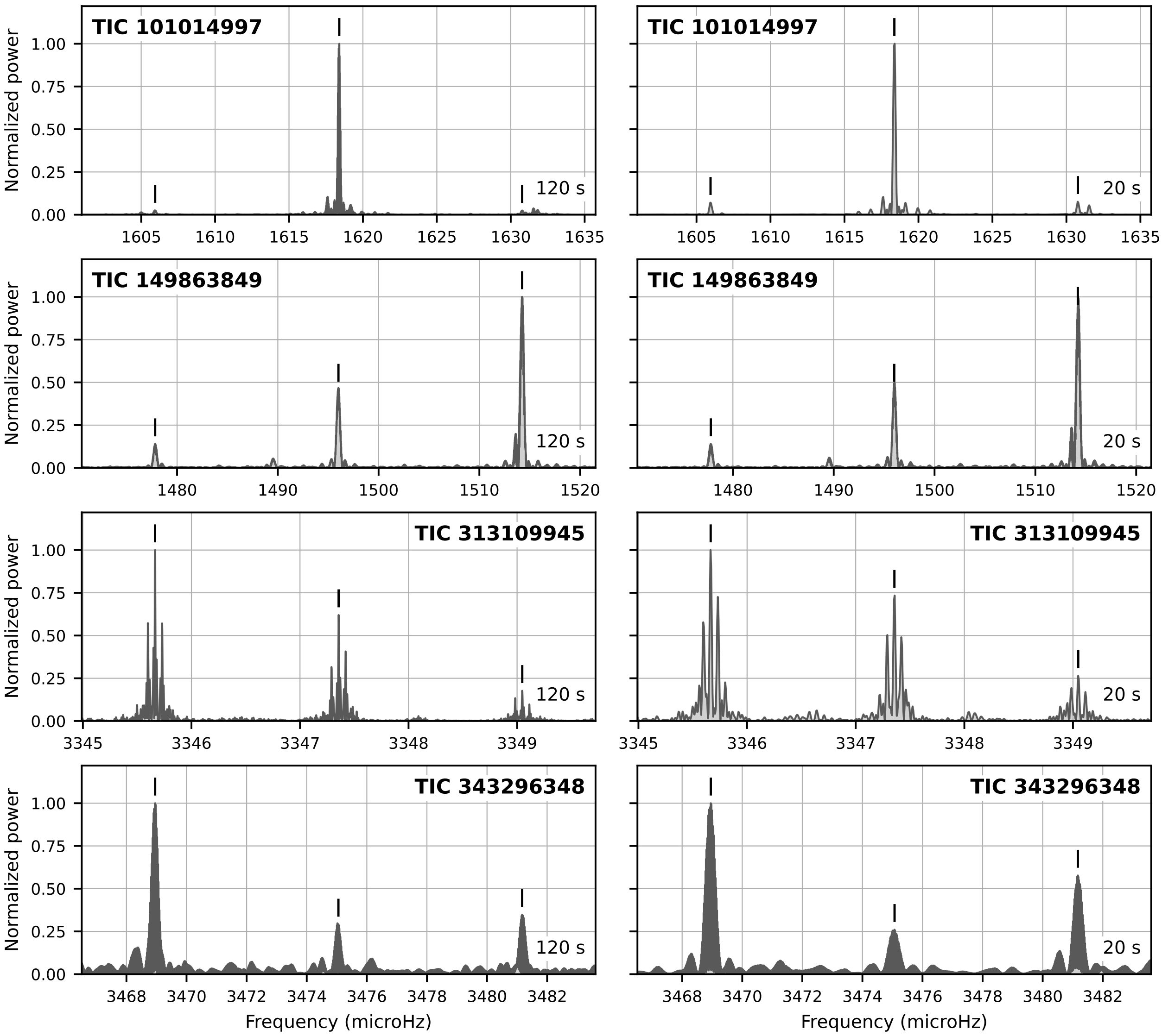

Fig. 4. Periodograms of the accepted rotationally split triplet candidates. Each row shows one ZZ Ceti star, with the 120 s and 20 s cadence data shown in separate columns where available. The frequency scale is given in μHz, and the periodogram power is normalised independently in each panel. Short vertical black markers above the peaks indicate the selected triplet components, after retaining only the highest-amplitude peak among nearby alternatives.

5.1. Discussion of Rotation

The automated search described above was designed to make the identification of rotationally split triplets reproducible across a heterogeneous TESS data set. Nevertheless, the number of accepted triplet candidates is modest: we retained 11 stars out of 239 TESS-observed ZZ Ceti targets, corresponding to an apparent detection efficiency of only 4.6 percent for the strict identification of complete triplets. If all objects with automated triplet candidates are counted before visual validation, the fraction is 30 out of 239 targets, or 12.6 percent. These numbers should not be interpreted as the intrinsic occurrence rate of rotational splitting among DAVs. They instead describe the efficiency with which complete, sufficiently clean triplet patterns can be recovered from the available TESS light curves using our conservative criteria. Several observational and methodological effects reduce this efficiency.

First, rotational splitting can only be recognised when at least three components of the same mode are detected with sufficient signal-to-noise ratio and frequency resolution. Many ZZ Ceti stars show only a small number of significant peaks in the TESS bandpass, while in others one or two components of a multiplet may fall below the detection threshold because of geometric cancellation, amplitude variability, or the inclination of the pulsation axis. In such cases the star may still be rotating at a measurable rate, but the available data do not contain a complete triplet. This is why we also generated doublet candidates as a diagnostic product, although we did not use doublets alone for the rotation-period determinations presented here. There is only one object, TIC 313109945, where an additional doublet at a different frequency range shows the same splitting within the frequency resolution, providing supporting evidence for the inferred rotational separation.

Second, the time coverage is highly non-uniform. Some targets were observed in many sectors, while others have only one or a few sectors of data. Shorter time bases reduce the Rayleigh frequency resolution and make it more difficult to separate close multiplet components. This particularly affects slowly rotating stars, for which the expected splittings are small. Con-

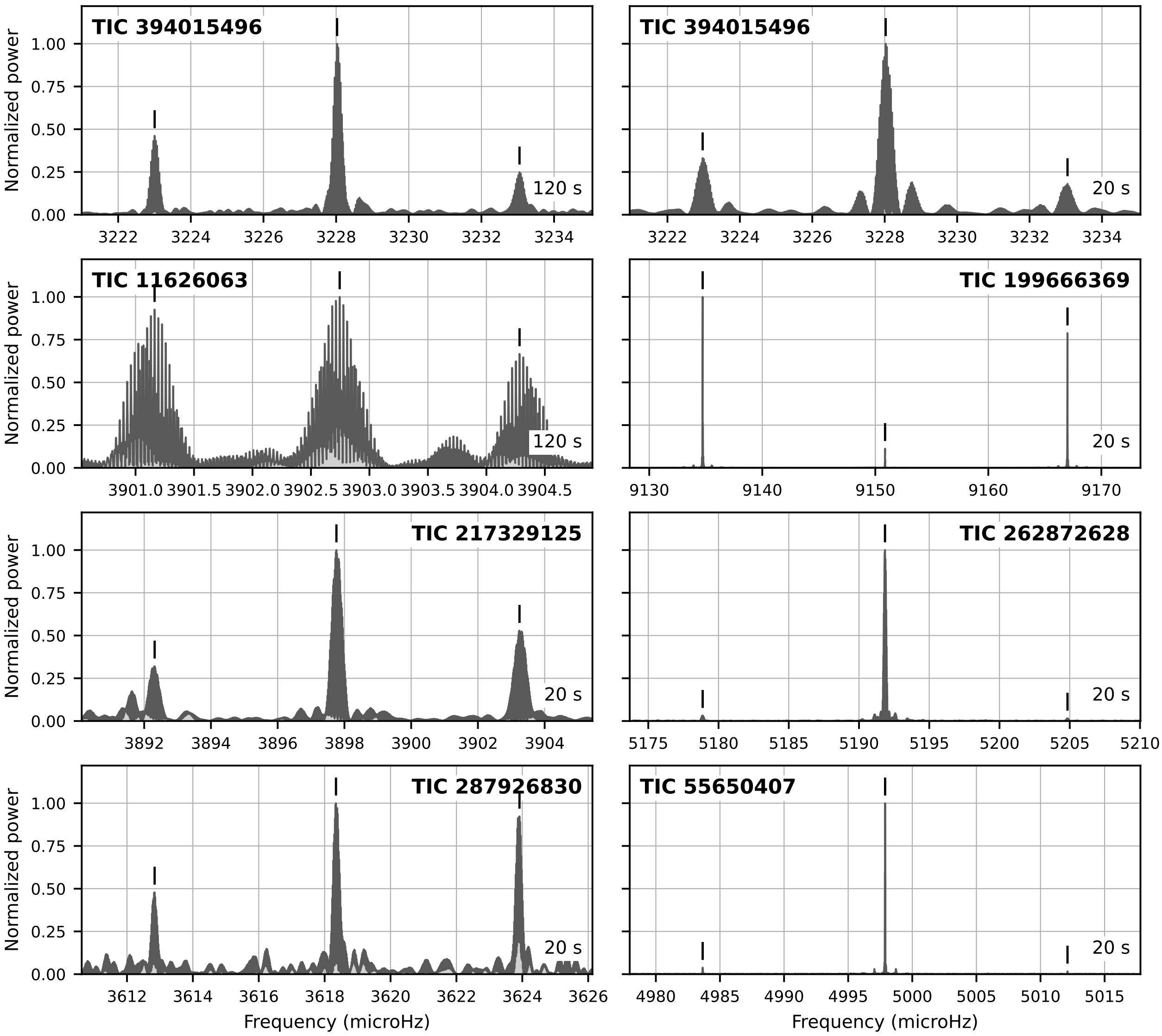

Fig. 5. Same as Fig. 4, but for the remaining accepted triplet candidates.

Table 4. Log of the TESS observations in which outburst-like brightenings were detected. Start times are given as BJD −2457000. The number of points and the time base refer to the corrected sector light curves used in the analysis. For targets with multiple entries, the TIC ID is listed only in the first row.

TIC ID	Cad. (s)	Sector	Start time	N	ΔT (d)	G (mag)	CROWDSAP
0001116746	120	48	2609.857	14931	26.13	16.467	0.803
67441210	120	20	1842.509	16016	26.32	15.823	0.672
101901770	120	64	3041.289	16698	24.75	16.093	0.771
219442838	20	63	3015.228	99445	24.51	16.415	0.189
	20	90	3747.164	97018	25.73	16.415	0.178
	120	9	1544.323	15294	24.16	16.415	0.186
	120	63	3015.228	16552	24.46	16.415	0.189
	120	90	3747.166	16089	25.72	16.415	0.178
307908863	20	48	2610.418	87422	25.57	15.559	0.138
366681966	120	72	3262.249	14274	23.32	14.980	0.983
630426257	120	70	3208.600	14432	24.39	16.955	0.435
800153845	20	44	2500.363	89161	24.08	17.322	0.123
	120	44	2500.366	14910	24.07	17.322	0.123
	120	61	2963.923	14806	23.83	17.322	0.145
800562727	120	44	2500.367	14737	24.07	17.702	0.343
842051075	120	62	2989.520	15551	24.64	18.232	0.191
1103347368	20	51	2698.355	39187	19.19	15.829	0.124
	120	51	2698.360	6499	19.18	15.829	0.124

Table 5. Outburst candidates identified in the corrected TESS light curves, listed event by event. The effective temperatures and surface gravities are the hydrogen-atmosphere photometric solutions from the Gaia EDR3 white dwarf catalogue. For targets with multiple events, the TIC ID and stellar parameters are listed only in the first row. Peak times are given as BJD −2457000, durations were measured from the smoothed light curves, and peak fluxes are the largest smoothed excesses relative to the local baseline.

TIC ID	$T_{\rm eff}$ (K)	log g (cgs)	Cadence	Peak time (BJD)	Duration (hr)	Peak flux (%)
0001116746	12127	8.04	120 s	2620.369	1.16	0.62
67441210	11610	8.09	120 s	1848.799	0.90	0.41
101901770	10816	8.02	120 s	3061.819	1.00	0.62
219442838	11609	8.01	120 s	1548.335	0.41	0.63
			20 s	3018.921	0.47	3.90
			120 s	3018.924	0.75	2.58
			120 s	3028.561	0.41	0.69
			20 s	3756.060	0.23	1.14
			120 s	3756.062	0.41	0.80
307908863	12042	8.03	20 s	2612.149	0.33	0.88
366681966	10936	8.01	120 s	3282.064	1.01	0.24
630426257	12258	7.85	120 s	3224.991	0.84	2.23
800153845	10502	7.90	120 s	2518.442	1.56	4.48
			20 s	2518.447	1.12	4.59
			120 s	2970.274	1.31	3.84
800562727	11724	7.97	120 s	2523.188	1.86	4.70
842051075	11830	8.00	120 s	2998.190	1.56	8.34
1103347368	10250	7.75	120 s	2715.217	1.23	0.86
			20 s	2715.217	0.76	0.84

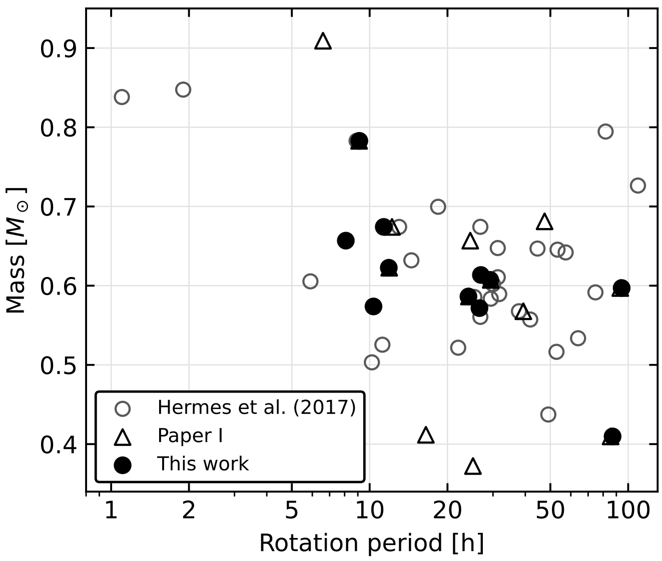

Fig. 6. Stellar mass as a function of rotation period for the ZZ Ceti stars with accepted triplet frequency structures. Filled black circles show the objects analysed in this work, open triangles show the Paper I rotators, and open circles show the comparison objects from Hermes et al. (2017) for which Gaia EDR3 white dwarf catalogue masses are available. All masses are the hydrogen-atmosphere photometric solutions from the Gaia EDR3 white dwarf catalogue. The horizontal axis is logarithmic.

versely, very dense frequency spectra can also be problematic: cool DAVs often show amplitude and frequency variability, unresolved close peaks, and possible combination frequencies, all of which can generate many formally acceptable frequency triples. The ranking and consensus-clustering steps reduce this problem but cannot eliminate it completely.

The main false-positive mechanisms for triplet candidates are therefore accidental near-equidistant frequency combinations, unresolved amplitude or frequency modulation, aliases produced by the observing window, and combination frequencies that mimic symmetric structures. Additional caution is required for frequency lists that reached the maximum prewhitening limit, because these objects may have complex residual spectra in which chance alignments become more likely. For this reason, the automated stage was used only to generate and rank candidates. The final sample was restricted to cases where the proposed triplet structure remained plausible after inspection of the frequency-amplitude diagrams, zoomed periodograms, and the consistency of the inferred splittings.

A natural interpretation of the detected triplet patterns is that they correspond to rotationally split components of $\ell = 1$ nonradial pulsation modes. Once the frequency separation between the components, $\delta\nu$, is measured, it can be used to estimate the stellar rotation period.

In the limit of slow rotation, the first-order frequency shift of a non-radial mode is given by

$$\delta\nu_{k,\ell,m} = m(1 - C_{k,\ell})\Omega, \tag{1}$$

where k, ℓ, and m denote the radial order, spherical degree, and azimuthal order of the pulsation mode, respectively. The quantity $C_{k,\ell}$ is the Ledoux constant, which approaches $C_{k,\ell} \approx 1/[\ell(\ell+1)]$ for high-overtone ($k \gg \ell$) g-modes, and Ω is the uniform rotation frequency.

As noted, for example, by Hermes et al. (2017), the observed doublet and triplet components in DAV stars cannot always be assumed to originate from high-overtone modes. To allow a direct comparison with the rotation rates reported by Hermes et al. (2017), we therefore adopted a uniform value of $C_{k,\ell} = 0.47$ when estimating the rotation periods of all stars in our sample.

We do not quote formal uncertainties for the derived rotation periods. The statistical uncertainty of a rotation period follows directly from the uncertainty of the measured splitting, if $C_{k,\ell}$ is kept fixed. In practice, however, the dominant uncertainties are not purely statistical: they are set by the frequency res-

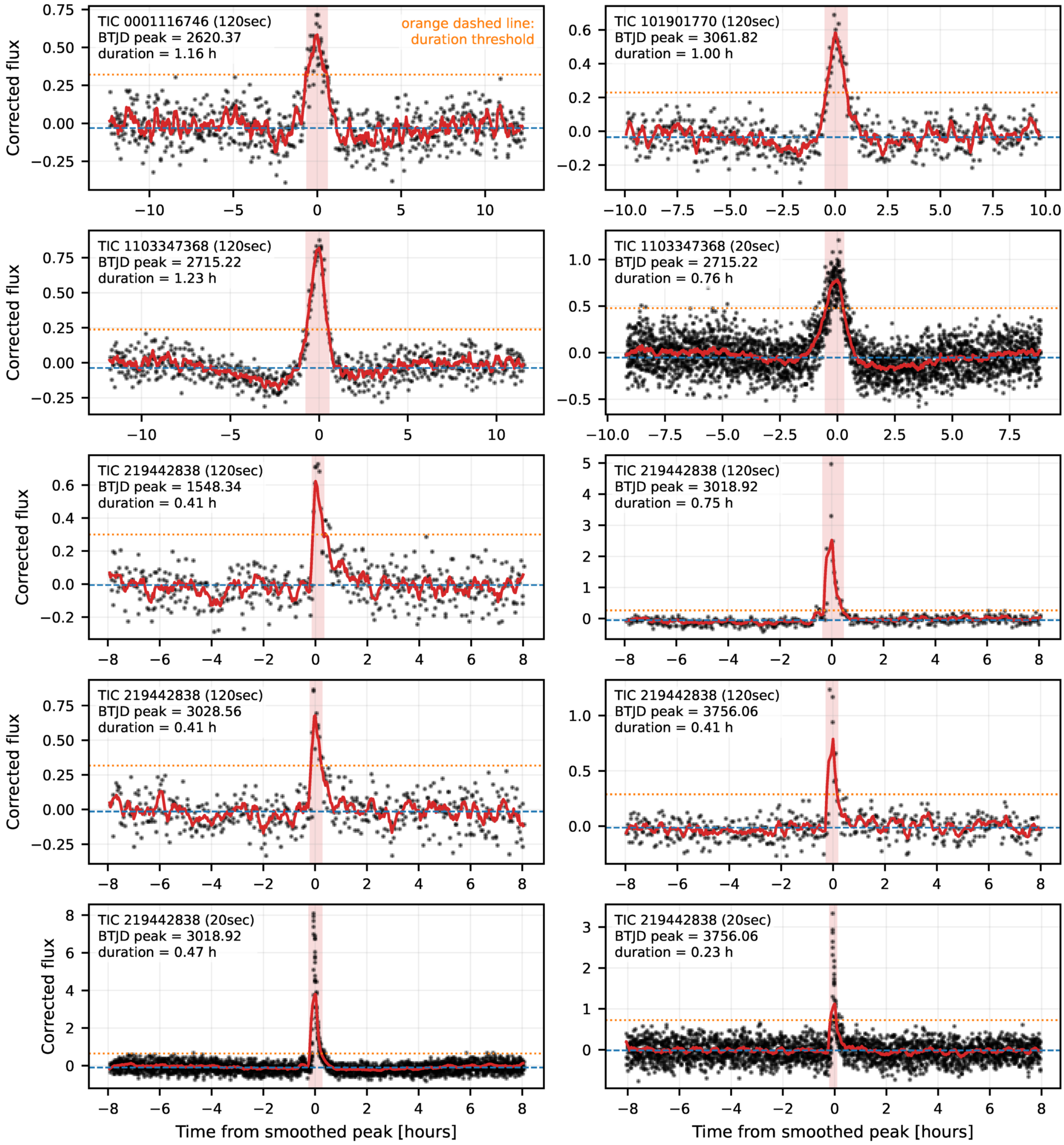

Fig. 7. Outburst-like brightenings detected in the corrected TESS light curves of ZZ Ceti stars. Each panel shows the flux variation around an individual candidate event, centred on the peak of the smoothed light curve. Grey points denote the corrected TESS fluxes, while the black curve shows the smoothed light curve used to estimate the event duration. The horizontal dashed line marks the duration threshold relative to the local baseline. The measured duration and the BJD time of the maximum brightness are indicated in each panel.

olution of the TESS data, possible amplitude or frequency variability, the identification of the correct triplet components, and the assumed value of the Ledoux constant. The periods listed in Table 3 should therefore be regarded as estimates based on the measured mean splittings rather than as values with formal error bars.

5.2. Discussion of Outbursts

The outburst search is subject to a different set of biases. TESS provides long, homogeneous light curves, but the large pixel size, flux dilution, sector gaps, and target-to-target differences in contamination can strongly affect the detectability of low-amplitude brightenings. A genuine outburst may be missed if only its low-amplitude onset or decay is present in the data, if it occurs during a gap, or if it is diluted by nearby sources. Conversely, false positives may be produced by residual instrumental trends, imperfect detrending near sector boundaries, scattered-light features, contaminant background stars, or short-lived excursions caused by imperfectly removed outliers.

These limitations are particularly relevant for the short durations measured for several of our outburst candidates. Our dura-

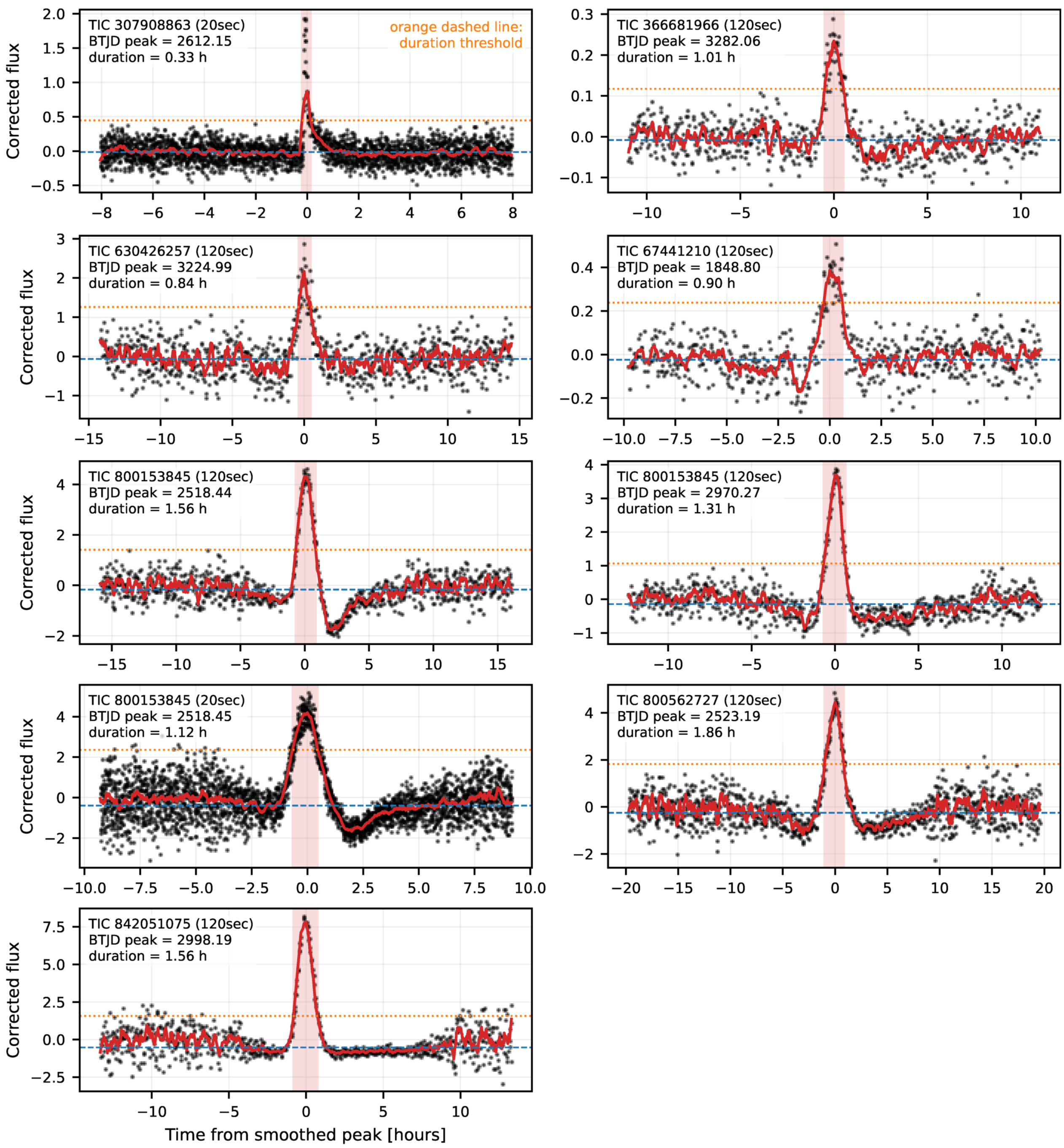

Fig. 8. Continuation of Fig. 7. Same as in Fig. 7, but for the remaining outburst candidates. The panels show the corrected TESS fluxes around the selected brightening events, together with the smoothed light curves and the adopted duration thresholds used to estimate the outburst durations.

tion estimates are based on the interval over which the smoothed light curve remains above a local threshold and therefore trace the high-confidence part of each event rather than necessarily the full physical outburst profile. This conservative definition helps avoid overestimating events affected by residual trends, but it can shorten the measured durations compared with studies based on higher signal-to-noise light curves or different duration definitions. For this reason, we refer to these detections as outburst candidates and emphasise the need for independent follow-up photometry and spectroscopic atmospheric parameters.

Despite these caveats, the conservative approach is appropriate for the present goal. The triplet search prioritises robust rotation-period estimates over completeness, while the outburst search prioritises reliable candidate identification over an exhaustive occurrence-rate measurement. The resulting samples are therefore best regarded as high-confidence subsets of a larger population of possible multiplet and outburst-like behaviour in TESS-observed ZZ Ceti stars.

Comparing our outburst candidates, summarised in Table 5, with the sample presented by Bell et al. (2017) in their Table 1, we find two notable differences. First, some of our candidates have higher effective temperatures than expected from the previously known outbursting ZZ Ceti stars, which were found close to the red edge of the empirical instability strip. If confirmed, this may indicate that outburst-like behaviour can occur over a wider temperature range than previously assumed. However, we note that our effective temperatures are taken from the photometric Gaia EDR3 white dwarf catalogue solutions; therefore, spectroscopic confirmation would be desirable.

Second, the durations of the candidate events identified in our TESS light curves are generally shorter than those reported by Bell et al. (2017). This difference may reflect intrinsic diversity among outbursting DAVs, but it may also be affected by the detection and measurement procedure, the smoothing timescale adopted here, the shorter or interrupted TESS observing windows, and the lower signal-to-noise ratio of some events. Therefore, we consider these objects as outburst candidates and treat the inferred durations as approximate estimates.

6. Summary and conclusions

We analysed TESS short- and ultrashort-cadence observations of a sample of known ZZ Ceti stars, using all available data up to Sector 96. Our goal was twofold: to search for rotationally split pulsation multiplets suitable for estimating stellar rotation periods and to identify possible outburst-like brightenings in the corrected light curves.

After downloading and correcting the available TESS light curves, we performed frequency analysis and iterative prewhitening on the merged data sets. We then searched the resulting frequency lists with an automated consensus-clustering pipeline designed to identify and rank closely spaced, approximately equidistant triplet structures before final visual validation. Out of 417 analysed frequency lists, 44 contained automated triplet candidates, corresponding to 30 TIC targets; 11 stars survived the final visual validation and were accepted as rotators. This corresponds to 4.6 percent of the 239 TESS-observed targets, but this value reflects the detection efficiency for clean, complete triplets rather than the intrinsic fraction of rotating ZZ Ceti stars. Assuming first-order rotational splitting and adopting $C_{k,\ell} = 0.47$, we derived rotation periods from the mean frequency separations. For objects with both 120 s and 20 s cadence detections, we averaged the splittings from the two data sets before calculating a single rotation period.

The resulting rotation periods span from about 8 h to 94 h. Most of the targets fall within the mass range typical of ZZ Ceti stars, and our sample does not contain very high-mass white dwarfs. A comparison with the literature compilation of Hermes et al. (2017) shows that our objects are broadly consistent with the large dispersion in rotation periods observed among normal-mass pulsating white dwarfs. The previously suggested tendency for the most massive white dwarfs to rotate faster is therefore not strongly tested by our sample.

We also searched the corrected TESS light curves for outburst-like brightenings. After automatic candidate selection and visual inspection, we retained 11 stars showing possible outburst events. The measured events are generally short, with median durations typically around or below two hours. When compared with the known outbursting DAVs discussed by Bell et al. (2017), our candidates appear to show two notable differences: some are hotter than expected for classical outbursting ZZ Ceti stars near the red edge of the instability strip, and the detected events are shorter in duration. These differences may indicate a broader range of outburst-like behaviour among DAVs, but they may also be influenced by the TESS sampling, data quality, detrending, and the adopted detection criteria. Spectroscopic atmospheric parameters and independent follow-up photometry would be valuable for confirming the nature of these candidates.

In summary, our analysis expands the set of TESS-observed ZZ Ceti stars with candidate rotationally split triplets and provides new rotation-period estimates for 11 objects. In addition, we identify 11 stars showing outburst-like behaviour, several of which may merit further investigation. The results demonstrate the continued value of extended TESS coverage for studying both the internal rotation and the nonlinear photometric behaviour of pulsating white dwarfs.

Acknowledgements. ZsB and ÁS acknowledge the financial support of the KKP-137523 'SeismoLab' Élvonal grant of the Hungarian Research, Development and Innovation Office (NKFIH). This paper includes data collected with the TESS mission, obtained from the MAST data archive at the Space Telescope Science Institute (STScI). Funding for the TESS mission is provided by the NASA Explorer Program. STScI is operated by the Association of Universities for Research in Astronomy, Inc., under NASA contract NAS 5–26555.

References

Bell, K. J., Hermes, J. J., Bischoff-Kim, A., et al. 2015, ApJ, 809, 14
Bell, K. J., Hermes, J. J., Montgomery, M. H., et al. 2016, ApJ, 829, 82
Bell, K. J., Hermes, J. J., Montgomery, M. H., et al. 2017, in Astronomical Society of the Pacific Conference Series, Vol. 509, 20th European White Dwarf Workshop, ed. P.-E. Tremblay, B. Gaensicke, & T. Marsh, 303
Bognár, Z. & Sódor, A. 2016, Information Bulletin on Variable Stars, 6184, 1
Bognár, Z. & Sódor, Á. 2024, A&A, 684, A76
Bognár, Z., Sódor, Á., Clark, I. R., & Kawaler, S. D. 2023, A&A, 674, A204
Brickhill, A. J. 1991, MNRAS, 251, 673
Córsico, A. H., Althaus, L. G., Miller Bertolami, M. M., & Kepler, S. O. 2019, A&A Rev., 27, 7
Dolez, N. & Vauclair, G. 1981, A&A, 102, 375
Gentile Fusillo, N. P., Tremblay, P.-E., Cukanovaite, E., et al. 2021, MNRAS, 508, 3877
Goldreich, P. & Wu, Y. 1999, ApJ, 511, 904
Hermes, J. J., Gänsicke, B. T., Kawaler, S. D., et al. 2017, ApJS, 232, 23
Hermes, J. J., Montgomery, M. H., Bell, K. J., et al. 2015, ApJ, 810, L5
Jenkins, J. M., Twicken, J. D., McCauliff, S., et al. 2016, in Proc. SPIE, Vol. 9913, Software and Cyberinfrastructure for Astronomy IV, 99133E
Kawaler, S. D. 2003, arXiv e-prints, astro
Kawaler, S. D. 2015, in Astronomical Society of the Pacific Conference Series, Vol. 493, 19th European Workshop on White Dwarfs, ed. P. Dufour, P. Bergeron, & G. Fontaine, 65
Luan, J. & Goldreich, P. 2018, ApJ, 863, 82
Montgomery, M. H., Hermes, J. J., Winget, D. E., Dunlap, B. H., & Bell, K. J. 2020, ApJ, 890, 11
Romero, A. D., Kepler, S. O., Hermes, J. J., et al. 2022, MNRAS, 511, 1574
Romero, A. D., Kepler, S. O., Oliveira da Rosa, G., & Hermes, J. J. 2025, ApJ, 984, 112
Winget, D. E., van Horn, H. M., Tassoul, M., et al. 1982, ApJ, 252, L65